

Article

Analysis of the Error in Retrievals of Aerosol Optical Properties from Sunphotometer Measurements of CARSNET Due to a Variety of Objective Factors

Ke Gui ^{1,2}, Huizheng Che ^{2,*}, Quanliang Chen ^{1,*}, Jie Yu ^{1,2}, Yu Zheng ^{2,3}, Sai Lu ⁴, Hong Wang ², Yaqiang Wang ², Xiaoye Zhang ² and Guangyu Shi ⁵

Received: 5 December 2015; Accepted: 8 January 2016; Published: 13 January 2016

Academic Editors: Gabriele Curci and Giovanni Pitari

¹ College of Atmospheric Science, Chengdu University of Information Technology, and Plateau Atmospheric and Environment Laboratory of Sichuan Province, Chengdu 610225, China; gkcu@163.com (K.G.); yujiesunshine@163.com (J.Y.)

² State Key Laboratory of Severe Weather (LASW) and Institute of Atmospheric Composition, Chinese Academy of Meteorological Sciences, Beijing 100081, China; hblfzhengyu@126.com (Y.Z.); wangh@cma.gov.cn (H.W.); wangyq@camsma.cn (Y.W.); xiaoye@camsma.cn (X.Z.)

³ Key Laboratory for Aerosol-Cloud-Precipitation of China Meteorological Administration, Nanjing University of Information Science and Technology, Nanjing 210044, China

⁴ Meteorological Observation Center, China Meteorological Administration, Beijing 100081, China; lusai0802@foxmail.com

⁵ State Key Laboratory of Numerical Modeling for Atmospheric Sciences and Geophysical Fluid Dynamics (LASG), Institute of Atmospheric Physics, Chinese Academy of Sciences, Beijing 100029, China; shigy@mail.iap.ac.cn

* Correspondences: chehz@camsma.cn (H.C.); chenql@cuit.edu.cn (Q.C.); Tel.: +86-10-5899-3116 (H.C.); Fax: +86-10-6217-6414 (H.C.)

Abstract: *In situ* observation of the aerosol optical properties is important to the validations of satellite and modeling results; however, the operational measurements can be affected by some objective factors. An experiment study has been performed in order to analyze the error in retrievals of aerosol optical properties from sunphotometer measurements caused by a variety of *in situ* objective factors. The standard instrument relative error analysis method was used to determine the relative error of aerosol optical depth (AOD) and Ångström exponent (AE) under the effects of five factors: spider web inside the collimator (F1); collimator bending (F2); dust inside the optical head (F3); incrustation scale inside the optical head (F4); and dust and incrustation scale inside the optical head (F5). The results showed that the five factors caused error for AOD retrieved at 1020, 870, 670 and 440 nm, with the maximum error occurring at 870 nm due to the more sensitive measurement signals. The error ranges of AOD derived from the direct solar measurements in the four bands were -0.34% – 8.77% , -6.22% – 9.68% , -0.05% – 2.52% , -0.96% – 3.48% and 5.42% – 13.38% for F1, F2, F3, F4 and F5, respectively. The maximum error occurred under the influence of F5 with an average error value of 10%, while the minimum occurred owing to F3 with an average error value of 1%. All of the AEs retrieved from the experimental instruments were smaller than that from the reference instrument. The AE error values were 15.19%, 25.57%, 4.56%, 4.41% and 8.83% for F1, F2, F3, F4 and F5, respectively. The average AE retrieval error value was 11.7%.

Keywords: CE318 sunphotometer; aerosol optical depth (AOD); Ångström exponent; retrieval error

1. Introduction

Atmospheric aerosol generally refers to a variety of suspended solids and liquid particles of diameter less than 10 μm in the atmosphere [1,2]. On the one hand, aerosol particles play an important role in global and regional climate change, causing a wide range of heating and cooling effects, depending on how aerosol particles absorb and scatter solar radiation and change the energy budget of the Earth–atmosphere system [3,4]. On the other hand, aerosol particles can act as cloud condensation nuclei (CCN) and ice nuclei (IN) upon which cloud droplets and ice crystals form [5–8]. Furthermore, on regional scales and the global scale, aerosol particles cause reduced visibility and, regionally, contribute to changes in precipitation [9,10]. Recently, a large number of studies have indicated that clouds and the aerosol–cloud–radiation interactions contribute the largest uncertainty to assessments and interpretations of the Earth’s changing energy budget [11–17].

Satellite remote sensing and ground-based observation are the two most important ways for monitoring the Earth’s aerosol properties long-term [18]. In particular, to better study aerosol optical properties, microphysical properties, and validate satellite retrieval results, using a ground-based observation network is very effective and accurate [18]. So far, several ground-based networks have been established, including Cimel CE318 narrow band sunphotometers based networks of AERONET (Aerosol Robotic NETwork) [19] and PHOTONS (PHOtométrie pour le Traitement Opérationnel de Normalisation Satellitaire) [20], RIMA [21], AEROCAN [22], the SKYradiometer network (SKYNET) [23,24]. In addition, other relevant networks such as EARLINET [25], LALINET [26] and MPLNET [27] are providing vertical-resolved aerosol properties over different parts of the world. At present, around 40 AERONET/PHOTONS stations are located in China. However, only a few sites have continuous observation records [28,29]. The China Meteorological Administration (CMA) established the aerosol monitoring network CARSNET (China Aerosol Robot Sunphotometer Network) in 2002 for the study of dust aerosol optical properties over different areas in China and the validation of satellite retrievals [28]. CARSNET is an independent aerosol monitoring network that uses the same types of sunphotometers as AERONET. To date, the number of CARSNET stations has increased to more than 60. These stations are not only established by the CMA but also extend to local meteorological agencies, institutes, universities, and individual scientists throughout China [29]. The network already provides a long-term, continuous database of aerosol optical, microphysical and radiative properties for aerosol research and characterization, and validation of satellite retrievals [29–35].

The CE318 sunphotometer is appropriate for long-term field observation. However, long-term field observation is influenced by many factors, such as environmental conditions, human activity, and instrument loss/damage. These factors lower the measuring accuracy of the sunphotometer, thus affecting the retrieval accuracy of aerosol optical properties and also microphysical properties. To improve the precision of aerosol optical property retrievals, much research has been conducted on the calibration methods of the CE318 sunphotometer, including radiance calibration using a calibrated integrating sphere [30] and direction sun calibration using the Langley plot technique and intercomparison with reference instruments [28–31]. Recently, the aerosol data based on AERONET, PHOTONS, CARSNET and other observational networks have been extensively used in studies of atmospheric aerosol optical properties, climatic change, and other important topics [32–35]. However, owing to the particularity of field observation, some objective factors of influence are easily neglected—for instance, spider webs in the collimator not being cleaned in time, a lack of regular cleaning of the dust and incrustation scale (caused by raindrops on the lens of the optical head) inside the optical head, and the collimator itself being left uncorrected having become bent. These factors may result in errors in the retrieval of aerosol optical properties. To acquire accurate aerosol data, it is important to analyze the retrieval error of aerosol optical properties caused by these objective factors of influence.

As a valuable aerosol characteristic, optical depth is also a key parameter for various aerosol-related studies. It was applied to many fields, such as aerosol radiative forcing, atmospheric

corrections of the aerosol effect on remote sensing, *etc.* [36]. Holben [19] and Eck [37] pointed out that the total uncertainty in the aerosol optical depth (AOD) result from calibration uncertainty of V_0 and uncertainty in ozone and Rayleigh optical depth for field measurement is about 0.010 to 0.021 for the instrument with well maintenance and performance. The wavelength dependence of AOD and some basic information on the aerosol size distribution are commonly characterized by the Ångström exponent (AE) [37]. Wagner and Silva [38] calculated the maximum error for Ångström exponent under the conditions of clean and hazy respectively, by assuming some constant errors for AOD measurements at 440 nm and 870 nm. The results showed in low-AOD regimes that small uncertainties on AOD can propagate to large uncertainties in Ångström exponents.

In the present study, a reference instrument and two experimental instruments were used to investigate the objective factors of influence possibly causing error in the retrieval of aerosol optical properties. Relative error analysis was then used to calculate the relative error of aerosol optical depth (AOD) and the Ångström exponent (AE). The relative error of AOD and AE was analyzed for the instruments with good-calibration but abnormal performances caused by the objective factors of spider web inside the collimator, collimator bending, dust inside the optical head, incrustation scale inside the optical head, and dust and incrustation scale inside the optical head. In addition, the Ångström exponent error is verified based on errors for *in situ* AOD measurements. The progress with respect to past works of the present study is that five more objective impact factors of AOD measurement were analysed. These factors were not be considered previously, and they could obviously affect the ground-based *in situ* aerosol optical properties observation. The results of this work will be beneficial to us with eliminating the AOD measurements error and decrease its uncertainty caused by these factors in some degree. It also provides a scientific basis for improving the stability of operational instruments and the data reliability, thus helping to guarantee the accuracy of aerosol optical property retrievals.

2. Data and Analysis Method

2.1. Instruments and Measurement Data

The CE318 sunphotometer is a portable autonomous instrument. Its component parts include a robot, optical head, collimator, and control box [30]. The CE318 makes direct spectral solar radiation measurements within a 1.2° full field of view at about 15 min intervals in eight normal bands (340, 380, 440, 500, 675, 870, 1020 and 1640 nm) and one water vapor band (at 940 nm). The bandwidth of each channel is 10 nm. Measurements at 340, 380, 440, 500, 675, 870, 1020 and 1640 nm are used to calculate AOD, and measurements at 940 nm are used to retrieve columnar water vapor [19]. The aerosol particles in Beijing are typical urban aerosols. The particles mainly come from local emission such as vehicles and fugitive dust and regional transportation such as industry, biomass burning, and coal combustion *etc.* [39]. Typically, AOD decreases with increasing wavelength for urban pollution aerosols. Aerosol size distribution, refractive index, and single-scattering albedo can be obtained by using sky radiance almucantar measurements and direct sun measurements [40,41] as well as polarized radiances in the sun principal plane [40–42].

Three Cimel sunphotometers were set up on top of the Chinese Academy of Meteorological Sciences (116.317°E , 39.933°N , 105 m), including a reference instrument ($n^\circ 746$) and two experimental instruments ($n^\circ 433$ and $n^\circ 163$). The experiment was composed of five groups, each focused on one of five factors: spider webs; collimator bending; dust; incrustation scale; dust and incrustation scale. The experiment information is detailed in Table 1.

Table 1. Details of each experiment group.

| Factors | Spider Web | Collimator Bending | Dust | Incrustation Scale | Dust and Incrustation Scale |
|--------------------|---------------|--------------------|---------------|--------------------|-----------------------------|
| Instrument number | $n^\circ 163$ | $n^\circ 433$ | $n^\circ 433$ | $n^\circ 433$ | $n^\circ 433$ |
| Observation period | 2 days | 3 days | 2 days | 2 days | 2 days |
| Raw data | 54 | 120 | 90 | 56 | 63 |
| Valid data | 15 | 49 | 25 | 19 | 11 |

To obtain consistent data for comparison, the data of the two experimental instruments were selected on the basis of the reference instrument data time series. Only data within a minute between the experimental instruments and the reference instrument were used to retrieve AOD and AE and compare the error in optical properties between when the status of the instruments was “affected” (*i.e.*, affected by one of the experimental factors) and when it was “non-affected” (*i.e.*, not affected by any of the experimental factors).

2.2. Calibration

Three Cimel sunphotometers were calibrated to make the data more accurate and reliable. The reference instrument (n°746) is operated within both CARSNET and AERONET, and is calibrated using the PHOTONS calibration facility in Lille (LOA/USTL, France) and the Izaña Observatory (Tenerife, Spain), by the Langley plot technique following a calibration protocol method established in 2004 [20,28]. The experimental instruments (n°433 and n°163) were calibrated by the Langley plot method and the inter-comparison calibration method at least once a year following the AERONET calibration protocol [28]. During the inter-comparison calibration process, the AOD at 500 nm on the calibration day should be less than 0.20, and with little fluctuation [29]. The Langley plot technique is derived from the Beer–Lambert–Bouguer law:

$$V_{\lambda} = V_{0\lambda}R^{-2}exp(-m\tau) \tag{1}$$

where V_{λ} and $V_{0\lambda}$ are the output voltages of the sunphotometer and the top of the atmosphere, respectively; R^{-2} is a correction coefficient for the Sun–Earth distance; and m is the optical air masses with corresponding optical depth τ (m can be calculated according to the date, time, latitude and longitude of the location).

Taking the natural log of Equation (1):

$$\ln V_{\lambda} = \ln [V_{0\lambda}R^{-2}] - m\tau \tag{2}$$

When the atmospheric conditions are stable and clear, under the rectangular coordinate system with m as the x -axis and $\ln V_{\lambda}$ as the y -axis, and using a least-squares fit, the linear intercept is $\ln [V_{0\lambda}R^{-2}]$. The calibration value $V_{0\lambda}$ can then be calculated by the intercept. The uncertainty in AOD due to the uncertainty in $V_{0\lambda}$ for the reference instruments is better than 0.002–0.005 [19].

According to the weather conditions, the data of 29 October 2015 were chosen from the calibration of the two experimental instruments (n°433 and n°163) and, the calibration curve is shown in Figure 1. The minimum correlation coefficients of the calibration equation at 870 nm were 0.988 and 0.976 for n°163 and n°433, respectively, which met the needs of the experiment.

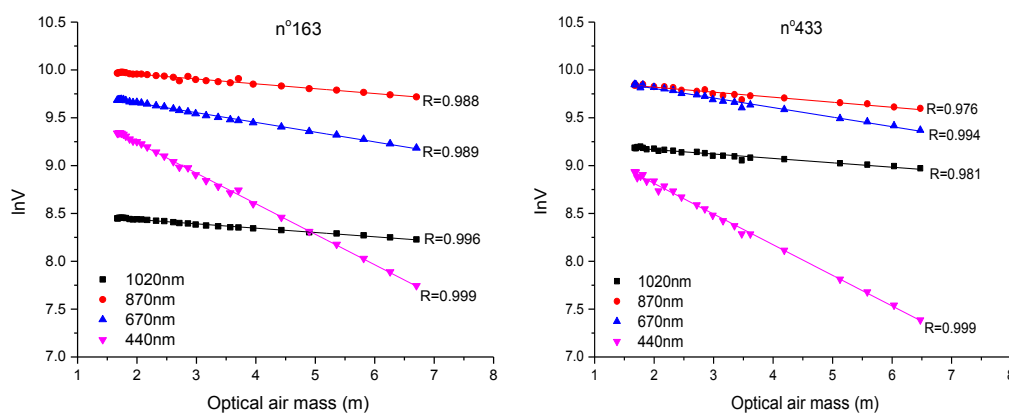


Figure 1. Calibration curves of the experimental instruments.

2.3. Calculation of Aerosol Optical Properties

2.3.1. Aerosol Optical Depth

The extraterrestrial solar radiation is attenuated by particles and molecules in the atmosphere through absorption and scattering. According to the Beer–Lambert–Bouguer attenuated law [19]:

$$I(\lambda) = \frac{I_0(\lambda)}{R^2} \exp(-m_r(\theta)\tau_r(\lambda) - m_{o_3}\tau_{o_3}(\lambda) - m_a(\theta)\tau_a(\lambda)) \quad (3)$$

where I is the measured irradiance (in arbitrary units), I_0 is a calibration constant; R is the Sun–Earth distance; m_r , m_{o_3} and m_a are the respective air masses for molecular scattering, ozone absorption and aerosol extinction with corresponding optical depths of $\tau_r(\lambda)$, $\tau_{o_3}(\lambda)$ and $\tau_a(\lambda)$; θ is the sun zenith angle; p is actual atmospheric pressure; and p_0 is standard atmospheric pressure.

AOD can be calculated using the following formula:

$$\tau_a(\lambda) = \frac{1}{m_a(\theta)} \left(\ln \frac{V(\lambda)}{V_0(\lambda)R^2} - m_r(\theta)\tau_r(\lambda) - m_{o_3}(\theta)\tau_{o_3}(\lambda) \right) \quad (4)$$

where $V(\lambda)$ is the observation value of the CE318 sunphotometer, $V_0(\lambda)$ is the calibration coefficient; and $m_a(\theta)$, $m_r(\theta)$ and $m_{o_3}(\theta)$ are calculated according to Equations (5)–(7) [43–45]:

$$m_a(\theta) = \frac{1}{\sin(e) + 0.0548 \times (e + 2.65)^{-1.452}} \quad (5)$$

$$m_r = \frac{1}{\sin(e) + 0.50572 \times (e + 6.07995)^{-1.6364}} \quad (6)$$

$$m_{o_3} = \frac{R + h}{\sqrt{(R + h)^2 - (R + h)^2 \times \cos^2(e)}} \quad (7)$$

where e is the solar elevation angle, R (6370 km) is the mean radius of Earth, r is the station height above sea level in km, and h (22 km) is the height of the ozone layer.

Rayleigh scattering optical depth is calculated using the following formula [46]:

$$\tau_r(\lambda) = 0.00864 \times \lambda^{-(3.916 + 0.074\lambda + \frac{0.050}{\lambda})} \times \frac{p}{1013.5} \quad (8)$$

The optical depth of ozone is calculated using the following formula:

$$\tau_{o_3}(\lambda) = a_{o_3}(\lambda) \times o_3 \times m_{o_3} \quad (9)$$

where $a_{o_3}(\lambda)$ is the absorption coefficient of ozone; o_3 is the quantity of ozone in the atmosphere in Dobson units (ozone content can be obtained from the monthly TOMS satellite climatology data); and m_{o_3} is the air mass of ozone.

2.3.2. Ångström Exponent

AE can be obtained by the well-known Ångström formula [47,48]:

$$\tau_a(\lambda) = \beta\lambda^{-\alpha} \quad (10)$$

where AE (α) is defined as a wavelength exponent, which can be used to reflect the characteristics of particle size. The AE can be calculated by the optical depth at the wavelengths of 440 nm and 870 nm for the Cimel sunphotometer:

$$\alpha = -\frac{\ln(\tau_a(440\text{ nm})/\tau_a(870\text{ nm}))}{\ln(440/870)} \quad (11)$$

2.4. Analysis Method

2.4.1. Relative Error Analysis Method of Aerosol Optical Depth

The reference instrument (n°746) has been running non-affected by non-desirable experimental factors during the experiment period. Taking experimental instrument n°433 as an example, when the status of the instrument (n°433) was “non-affected” (*i.e.*, none of the experimental factors is influencing the instrument’s operation), the AOD error at 1020 nm, 870 nm, 670 nm and 440 nm between the experimental instrument (n°433) and the reference instrument (n°746) was defined as $E1$:

$$E1 = (AOD_{433} - AOD_{746})/AOD_{746} \quad (12)$$

where AOD_{433} is the AOD for the experimental instrument (n°433) under the condition of the instrument running well (*i.e.*, its status was “non-affected”), and AOD_{746} is the AOD for the reference instrument (n°746).

When the status of the instrument (n°433) was “affected” (*i.e.*, one of the experimental factors was influencing the instrument’s operation), the AOD error at 1020 nm, 870 nm, 670 nm and 440 nm between the experimental instrument (n°433) and the reference instrument (n°746) was defined as $E2$:

$$E2 = (AOD^*_{433} - AOD_{746})/AOD_{746} \quad (13)$$

where AOD^*_{433} is the AOD for the experimental instrument (n°433) under the condition of the instrument running poorly (*i.e.*, its status was “affected”), AOD_{746} is the AOD for the reference instrument (n°746).

Considering $E1$ and $E2$, and excluding their self-generated error, the actual AOD error at 1020 nm, 870 nm, 670 nm and 440 nm caused by the experimental factor was defined as E :

$$E = (AOD^*_{433} - AOD_{433})/AOD_{433} \quad (14)$$

Combining Equations (12)–(14) yields a E of

$$E = (E2 - E1)/(E1 + 1) \quad (15)$$

where AOD^*_{433} is the AOD for the experimental instrument (n°433) under the condition of the instrument running poorly (*i.e.*, its status was “affected”), and AOD_{433} is the AOD for the experimental instrument (n°433) under the condition of the instrument running well (*i.e.*, its status was “non-affected”).

2.4.2. Relative Error Analysis Method of the Ångström Exponent

The AE relative error method was the same as that of AOD but with related definitions as follows:

$$S1 = (\alpha_{433} - \alpha_{746})/\alpha_{746} \quad (16)$$

$$S2 = (\alpha^*_{433} - \alpha_{746})/\alpha_{746} \quad (17)$$

$$S = (\alpha^*_{433} - \alpha_{433})/\alpha_{433} \quad (18)$$

$$S = (S2 - S1)/(S1 + 1) \quad (19)$$

where S_1 is the error of AE (α) between the experimental instrument ($n^\circ 433$) and the reference instrument ($n^\circ 746$) under the condition of the instrument's status being "non-affected", S_2 is the error of α between the experimental instrument ($n^\circ 433$) and the reference instrument ($n^\circ 746$) under the condition of the experiment instrument's status being "affected", and S is the actual error of α caused by the experimental factor.

Similarly, the actual error of the AOD and α of the experimental instrument ($n^\circ 163$) caused by the experimental factor could be obtained using the above methods.

3. Results and Discussion

3.1. Error Analysis of Aerosol Optical Depth

To obtain consistent data for comparison, the data of two experimental instruments were selected on the basis of the reference instrument data time series. Only the solar direct irradiance measurements data within a minute between the experimental instruments and the reference instrument were used to retrieve AOD. The calculated AODs are level 1.5 cloud-screened data, which eliminates the effect of clouds, according to the work of Smirnov [49]. CARSNET AOD measurements have the same accuracy as the AERONET/PHOTONS [28]. For the case when the status of all instruments was "non-affected", Figure 2 shows the variation trend of instantaneous AOD on 2 November. Figure 3a shows the daily mean and standard deviations of AOD at 1020 nm, 870 nm, 670 nm and 440 nm derived from the solar direct irradiance measurements of the experimental instrument ($n^\circ 163$) and the reference instrument ($n^\circ 746$) on 2 November. The daily mean values of AOD retrieved from $n^\circ 163$ were approximately 0.082 ± 0.017 , 0.105 ± 0.024 , 0.130 ± 0.038 and 0.256 ± 0.074 at 1020, 870, 670 and 440 nm, respectively. The daily mean values of AOD retrieved from $n^\circ 746$ were approximately 0.081 ± 0.019 , 0.103 ± 0.024 , 0.133 ± 0.039 and 0.259 ± 0.079 at 1020, 870, 670 and 440 nm, respectively. The daily mean values of AOD retrieved from the two instruments were basically the same. When compared to $n^\circ 746$, the daily mean of the AOD retrieved from $n^\circ 163$ was larger at 1020 nm and 870 nm but smaller at 670 nm and 440 nm. This could have been caused by the change in temperature. Figure 3b shows the daily mean and standard deviations of AOD at 1020 nm, 870 nm, 670 nm and 440 nm derived from the solar direct irradiance measurements of the experimental instrument ($n^\circ 433$) and the reference instrument ($n^\circ 746$) on 2 November. The daily mean values of AOD retrieved from $n^\circ 433$ were approximately 0.086 ± 0.018 , 0.107 ± 0.023 , 0.139 ± 0.036 and 0.269 ± 0.076 at 1020, 870, 670 and 440 nm, respectively. The daily mean values of AOD retrieved from $n^\circ 746$ were approximately 0.083 ± 0.019 , 0.106 ± 0.024 , 0.138 ± 0.039 and 0.269 ± 0.079 at 1020, 870, 670 and 440 nm, respectively. The daily mean AODs retrieved from the two instruments were basically the same. When compared to $n^\circ 746$, the daily mean AOD retrieved from $n^\circ 433$ was larger at 1020, 870, 670 and 440 nm—possibly caused by the loss of optical filter for $n^\circ 433$.

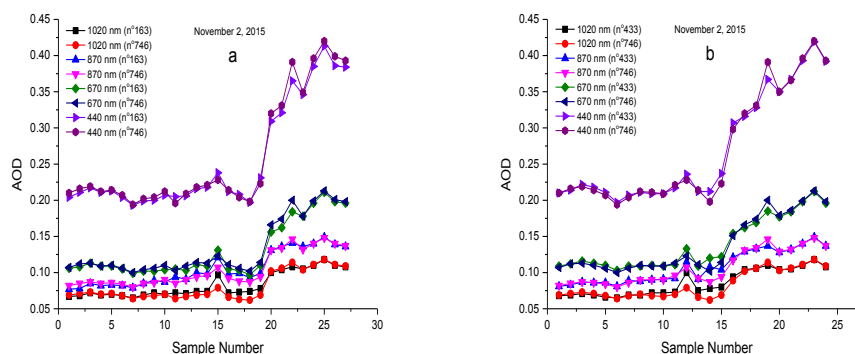


Figure 2. Comparison of the result of AOD retrieved at 1020 nm, 870 nm, 670 nm and 440 nm from the measurements of (a) $n^\circ 163$ and $n^\circ 746$; and (b) $n^\circ 433$ and $n^\circ 746$.

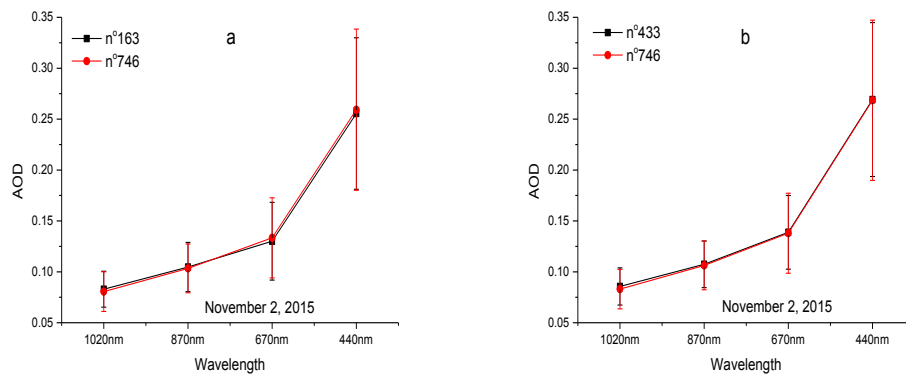


Figure 3. Daily mean and standard deviations of AOD at 1020 nm, 870 nm, 670 nm and 440 nm from the measurements of (a) n°163 and n°746; and (b) n°433 and n°746.

In the case of the instruments’ status being “non-affected”, $E1$ could be calculated according to Equation (12). Figure 4 and Table 2 show the $E1$ between experimental instrument n°163 and the reference instrument (n°746) was approximately 2.9%, 1.33%, -2.47% and -1.44% for 1020, 870, 670 and 440 nm, respectively. Meanwhile, the $E1$ between experimental instrument (n°433) and the reference instrument (n°746) were approximately 3.11%, 1.10%, 0.63% and 0.25% for 1020, 870, 670 and 440 nm, respectively. When compared to n°746, the maximum $E1$ between n°163 and n°746 occurred at 1020 nm with an error value of 2.9%, while the minimum occurred at 670 nm with an error value of -1.23% . The AOD at 1020, 870, 670 and 440 nm retrieved from n°433 was larger than that from n°746, and the error between n°433 and n°746 increased with increasing wavelength.

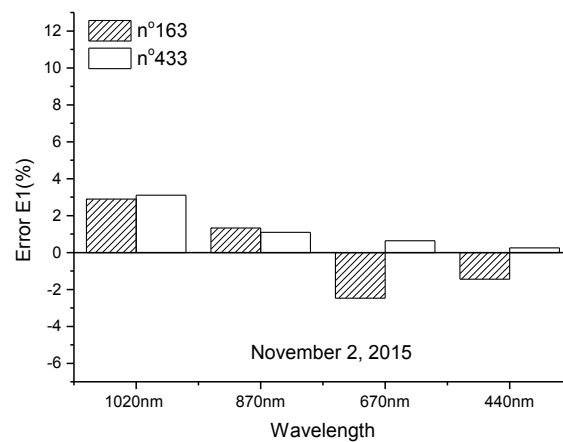


Figure 4. Error of AOD retrieved at 1020 nm, 870 nm, 670 nm and 440 nm between the experimental instruments and the reference instrument under the condition of the instruments’ status being “non-affected”.

Table 2. Error of the aerosol optical depth (AOD) retrieved at 1020 nm, 870 nm, 670 nm and 440 nm between the experimental instruments and the reference instrument.

| Wavelength (nm) | AOD Error (%) | | | | | | | | | | | | | | |
|-----------------|---------------|------|------|------|------|----------|-------|------|-------|-------|---------|-------|-------|-------|-------|
| | Error E1 | | | | | Error E2 | | | | | Error E | | | | |
| | F1 | F2 | F3 | F4 | F5 | F1 | F2 | F3 | F4 | F5 | F1 | F2 | F3 | F4 | F5 |
| 1020 | 2.90 | 3.11 | 3.11 | 3.11 | 3.11 | 7.32 | 10.90 | 4.24 | 2.12 | 15.88 | 4.30 | 7.55 | 1.10 | -0.96 | 12.39 |
| 870 | 1.33 | 1.10 | 1.10 | 1.10 | 1.10 | 10.21 | 10.89 | 3.64 | 4.62 | 14.63 | 8.77 | 9.68 | 2.52 | 3.48 | 13.38 |
| 670 | -2.47 | 0.63 | 0.63 | 0.63 | 0.63 | -4.73 | -4.67 | 0.80 | 0.15 | 9.57 | -2.32 | -5.27 | 0.17 | -0.48 | 8.88 |
| 440 | -1.44 | 0.25 | 0.25 | 0.25 | 0.25 | -1.78 | -5.98 | 0.20 | -0.14 | 5.68 | -0.34 | -6.22 | -0.05 | -0.39 | 5.42 |

In the case of the instruments' status being "affected", *i.e.*, one of the experimental factors was influencing the operation of the instrument, we performed five experiments for each of the five factors in turn (see Table 1 for further details) and, according to Equation (13), calculated the E_2 .

For convenience of description, we refer to the five factors using abbreviations as follows: spider web inside the collimator (F1); collimator bending (F2); dust inside the optical head (F3); incrustation scale inside the optical head (F4); dust and incrustation scale inside the optical head (F5). Figures 5 and 6 show the variation trend of AOD and the difference in AOD (δ_{AOD}) under the effects of five factors, respectively. It is clear that objective factors have a significant impact on the retrieval of AOD. The AOD measured by the experiment instrument has about -0.01 – 0.01 , -0.02 – 0.02 , -0.02 – 0.05 , -0.025 – 0.02 , and 0.02 – 0.05 difference from the results of the reference instrument for F1, F2, F3, F4, F5, respectively (Figure 6a–e). Some rapid upward fluctuations in AOD differences were probably caused by the Cimel sunphotometer sun tracking problem (Figure 6d). As shown in Figure 6f, it is clear that AODs measured at 870 nm by the experiment instrument have a biggest difference from the results of the reference instrument for all experiment factors. The average AOD difference that occurred at 870 nm is about 0.006, 0.006, 0.012, 0.027, and 0.037 between the reference instrument and experiment instrument for F1, F2, F3, F4 and F5, respectively. Figure 7 and Table 2 show for F1, compared to $n^{\circ}746$, the AOD retrieved at 1020 and 870 nm was larger but smaller at 670 nm and 440 nm. Furthermore, the maximum E_2 occurred at 870 nm with an error value of 10.21%, while the minimum occurred at 440 nm with an error value of -1.78% . For F2, the AOD retrieved at 1020 nm and 870 nm was larger, with the same error of about 10.89%, but smaller at 670 nm and 440 nm. The minimum E_2 occurred at 670 nm with an error value of -4.67% . For F3, the AOD retrieved at 1020, 870, 670 and 440 nm was larger, the maximum E_2 occurred at 1020 nm with an error value of 4.24%, while the minimum E_2 occurred at 440 nm with an error value of 0.20%. For F4, the AOD retrieved at 1020, 870 and 670 nm was larger but smaller at 440 nm, the maximum E_2 occurred at 870 nm with an error value of 4.62%, while the minimum E_2 occurred at 440 nm with an error value of -0.14% . Finally, for F5, the AOD retrieved at 1020, 870, 670 and 440 nm was bigger, the E_2 increased with increasing wavelength, the maximum E_2 occurred at 1020 nm with an error value of 15.88%, while the minimum E_2 occurred at 440 nm with an error value of 5.68%.

In the case of considering E_1 and E_2 , E was calculated according to Equation (15). Figure 8 and Table 2 show that, for F1, compared to when the instrument was running with a "non-affected" status, the AOD retrieved at 1020 and 870 nm was larger but smaller at 670 nm and 440 nm. Furthermore, the maximum E occurred at 870 nm with an error value of 8.77%, while the minimum E occurred at 440 nm with an error value of -0.34% . For F2, the AOD retrieved at 1020 and 870 nm was larger, but smaller at 670 nm and 440 nm. The maximum E occurred at 870 nm with an error value of 9.68%, while the minimum E occurred at 670 nm with an error value of -5.27% . For F3, the AOD retrieved at 1020, 870 and 670 nm was larger but smaller at 440 nm. The maximum E occurred at 870 nm with an error value of 2.52%, while the minimum E occurred at 440 nm with an error value of -0.05% . For F4, the AOD retrieved at 1020, 670 and 440 nm was smaller but larger at 870 nm. The maximum E occurred at 870 nm with an error value of 3.48%, while the minimum E occurred at 440 nm with an error value of -0.39% . Finally, for F5, the AOD retrieved at 1020, 870, 670 and 440 nm was larger, the error E increased with increasing wavelength, the maximum E occurred at 870 nm with an error value of 13.38%, while the minimum E occurred at 440 nm with an error value of 5.42%.

In conclusion, these five kinds of factors will cause error in the AOD retrieved at 1020, 870, 670 and 440 nm. The average error caused by F1, F2 and F5 is larger than that of F3 and F4. The maximum error occurs for F5 with an average value of 10%, while the minimum error occurs for F3 with an average error value of 1%. Compared with the AOD uncertainty result from calibration uncertainty for field measurement, the uncertainty caused by these objective factors is bigger [37]. Therefore, the error caused by a variety of objective factors in the process of retrievals of aerosol optical properties could not be ignored. Scheduled maintenance of the CE318 sunphotometers is absolutely necessary for improving the accuracy of AOD measurements.

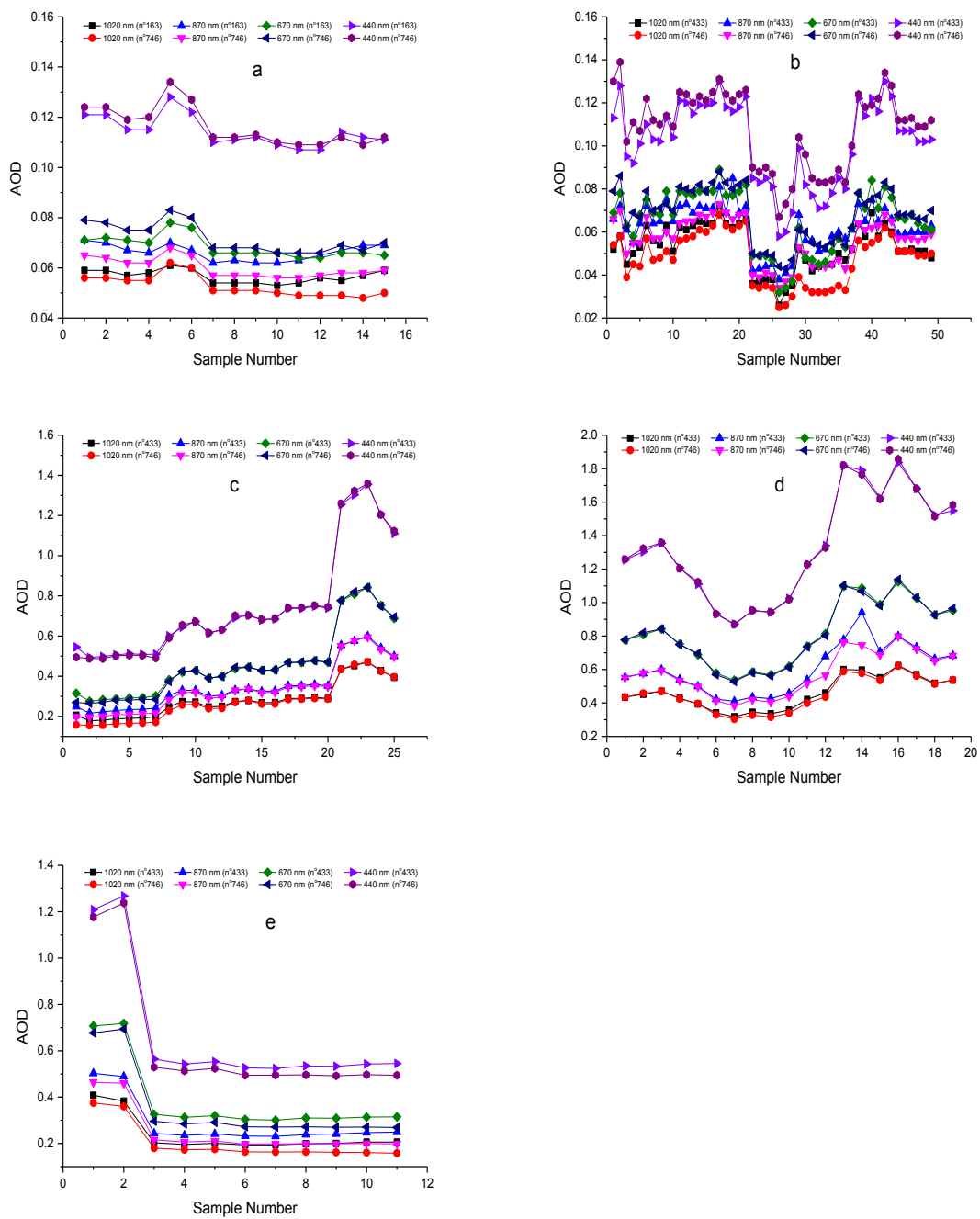


Figure 5. Comparison of the result of AOD retrieved at 1020 nm, 870 nm, 670 nm and 440 nm between the reference instrument and the experiment instruments under the effects of five factors: (a) spider web inside the collimator; (b) collimator bending; (c) dust inside the optical head; (d) incrustation scale inside the optical head; and (e) dust and incrustation scale inside the optical head.

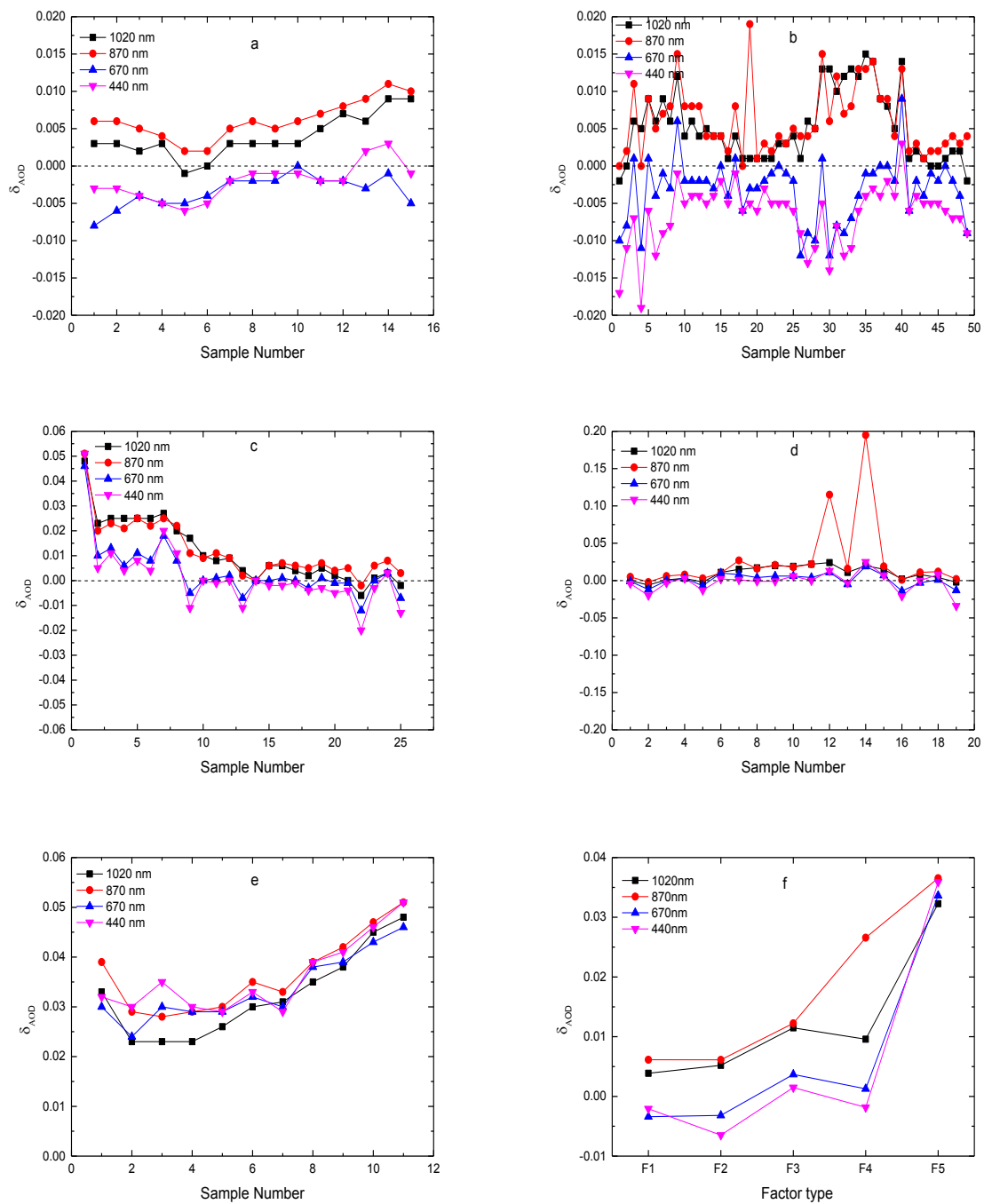


Figure 6. Simultaneously measured AOD differences between the reference instrument and the experiment instruments under the effects of five factors: (a) spider web inside the collimator; (b) collimator bending; (c) dust inside the optical head; (d) incrustation scale inside the optical head; and (e) dust and incrustation scale inside the optical head and (f) the averaged AOD differences under the effects of five factors.

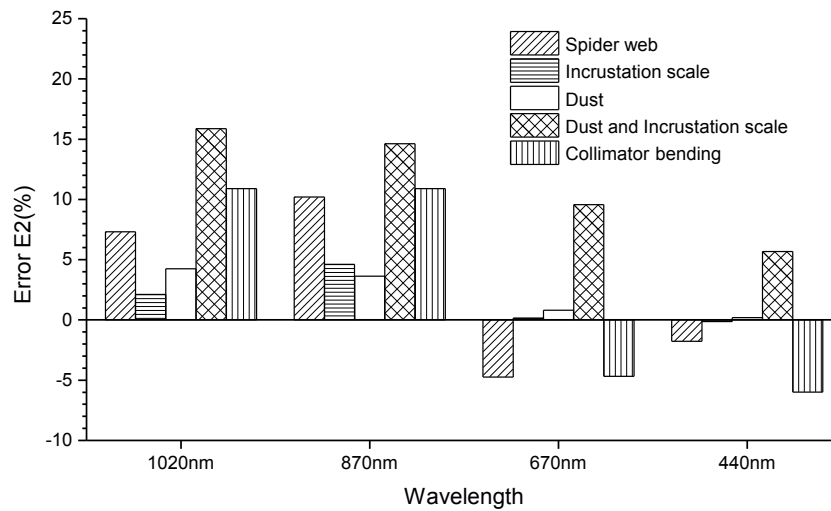


Figure 7. Error of AOD retrieved at 1020 nm, 870 nm, 670 nm and 440 nm between the experimental instruments and the reference instrument under the condition of the instruments’ status being “affected” (*i.e.*, affected by one of the factors indicated in the key).

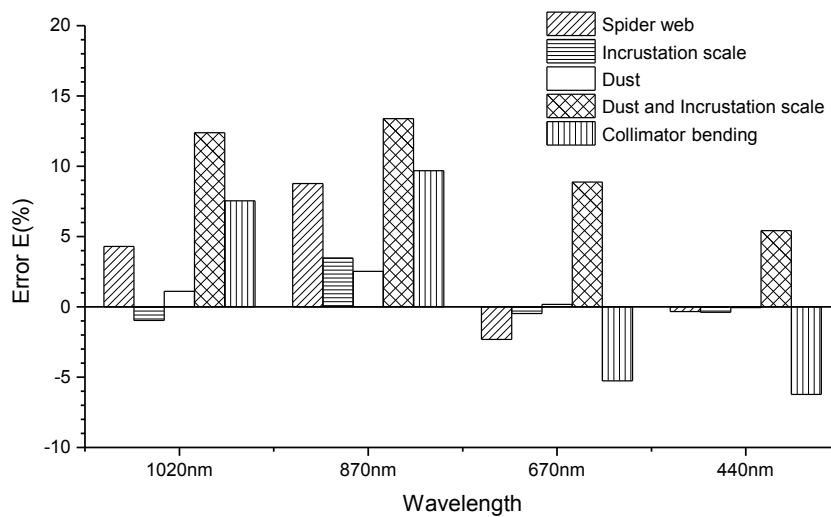


Figure 8. Actual error of AOD retrieved at 1020 nm, 870 nm, 670 nm and 440 nm between the experimental instruments and the reference instrument.

3.2. Error Analysis of Ångström Exponent

According to Equations (16)–(19), we calculated S_1 , S_2 and S . Figure 9 show the variation trend of AE and the difference in AE (δ_{AE}) under the effects of five factors. As shown in Figure 9, the AOD retrieval error caused by objective factors will bring some errors to the AE. The AE measured by the experiment instrument has about -0.25 – -0.10 , -0.50 – -0.09 , -0.20 – 0 , -0.33 – -0.01 , and -0.20 – -0.05 difference from the results of the reference instrument for F1, F2, F3, F4, F5, respectively (Figure 9). For the case of all instruments running well, *i.e.*, with a “non-affected” status, Figure 10 and Table 3 show that the AE retrieved from the two experimental instruments was smaller than that from the reference instrument ($n^{\circ}746$). The S_1 between experimental instrument $n^{\circ}163$ and the reference instrument ($n^{\circ}746$) was approximately -2.62% , while that between experimental instrument $n^{\circ}433$ and the reference instrument ($n^{\circ}746$) was about -0.80% . When the five factors were influencing the experimental instruments, the AE retrieved was smaller than that from the reference instrument. Furthermore, the maximum S_2 occurred for F2 with an error value of 26.17% , while the minimum

occurred for F4 with an error value of 5.18%. Finally, when considering S1 and S2, the AE retrieved from the two experimental instruments was smaller than that from the reference instrument. The actual maximum S occurred for F2 with an error value of 25.57%. This is expected as in low-AOD regimes small uncertainties on τ can propagate to large uncertainties on AE [38]. The minimum occurred for F4 with an error value of 4.41%.

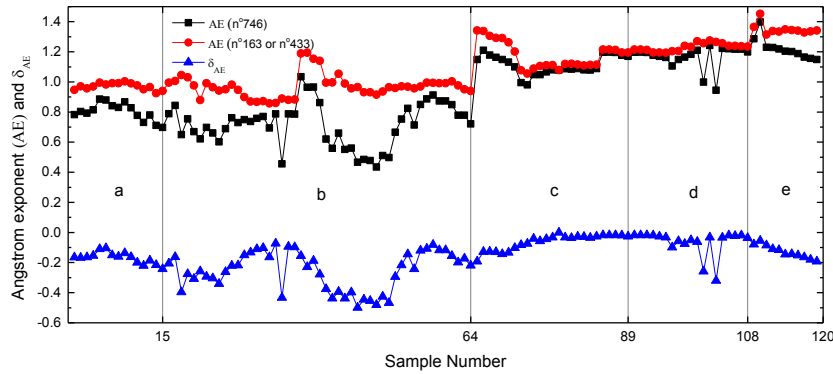


Figure 9. Simultaneously measured AE and AE differences between the reference instrument and the experiment instruments under the effects of five factors: (a) spider web inside the collimator; (b) collimator bending; (c) dust inside the optical head; (d) incrustation scale inside the optical head; and (e) dust and incrustation scale inside the optical head.

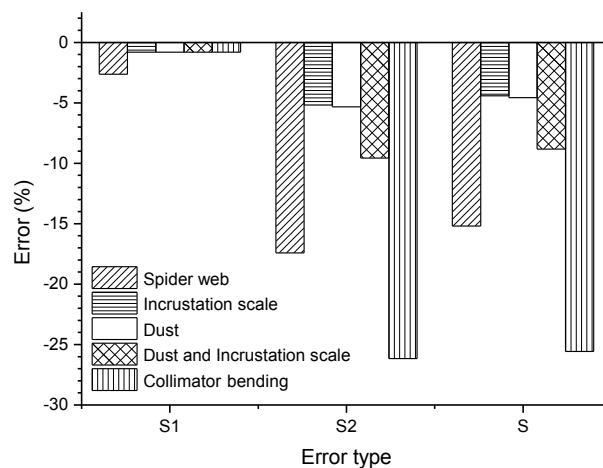


Figure 10. Error of the AE retrieved under the effect of different factors.

Table 3. Error of the Ångström exponent (AE) retrieved between the experimental instruments and the reference instrument.

| Error Type | AE Error (%) | | | | |
|------------|--------------|--------|-------|-------|-------|
| | F1 | F2 | F3 | F4 | F5 |
| S1 | -2.62 | -0.80 | -0.80 | -0.80 | -0.80 |
| S2 | -17.42 | -26.17 | -5.33 | -5.18 | -9.56 |
| S | -15.19 | -25.57 | -4.56 | -4.41 | -8.83 |

4. Conclusions

This study applied the relative error analysis method to analyze the relative error of AOD and AE under the effect of five factors: spider web inside the collimator (F1); collimator bending (F2); dust inside the optical head (F3); incrustation scale inside the optical head (F4); dust and incrustation scale

inside the optical head (F5). The main conclusions can be summarized as follows: the five factors caused error for AOD retrieved at 1020, 870, 670 and 440 nm, with the maximum occurring at 870 nm. The ranges of AOD retrieval error were -0.34% – 8.77% , -6.22% – 9.68% , -0.05% – 2.52% , -0.96% – 3.48% and 5.42% – 13.38% for F1, F2, F3, F4 and F5, respectively. The maximum error was caused by F5 with an average error value of 10%, while the minimum error was caused by F3 with an average error value of 1%.

The five factors also caused error for AE retrieval. The AOD distribution has important influence on Ångström exponent distribution. All of the AEs retrieved from the experimental instruments were smaller than that from the reference instrument. The AE error values were 15.19%, 25.57%, 4.56%, 4.41% and 8.83% for F1, F2, F3, F4 and F5, respectively. The average AE retrieval error value was 11.7%, with the actual maximum error caused by F2 and the minimum by F4.

This study shows that these objective factors can bring errors to the AOD retrieval at different wavelengths. The error caused by a variety of objective factors in the process of retrievals of aerosol optical properties could not be ignored. Scheduled maintenance of the CE318 sunphotometers is absolutely necessary for improving the accuracy of AOD measurements. However, the mechanism of how these objective factors affect the solar direct irradiance measurements still needs to be studied.

Acknowledgements: This work is financially supported by grants from the Project (41375153) supported by the National Natural Science Foundation of China, the National Key Project of Basic Research (2014CB441201), the Chinese Academy of Meteorological Sciences Basis Research Project (2014R17) and the Climate Change Special Fund of China Meteorological Administration (CCSF201504).

Author Contributions: Ke Gui wrote the article; Huizheng Che and Quanliang Chen conceived and designed the experiments; Ke Gui, Yu Zheng, and Sai Lu performed the experiments; Ke Gui and Jie Yu analyzed the data; Hong Wang, Yaqiang Wang, Xiaoye Zhang, and Guangyu Shi helped perform the statistical analysis.

Conflicts of Interest: The authors declare no conflict of interest.

References

1. Zhang, X.Y. Aerosol over China and their climate effect. *Adv. Earth Sci.* **2007**, *22*, 12–16.
2. Shi, G.Y.; Wang, B.; Zhang, H.; Zhao, J.Q.; Tan, S.C.; Wen, T.X. The radiative and climatic effects of atmospheric aerosols. *Chin. J. Atmos. Sci.* **2008**, *32*, 826–840.
3. Charlson, R.J.; Schwartz, S.E.; Hales, J.M.; Cess, R.D.; Coakley, J.A.; Hansen, J.E.; Hofmann, D.J. Climate forcing by anthropogenic aerosols. *Science* **1992**, *255*, 423–430. [[CrossRef](#)] [[PubMed](#)]
4. Hansen, J.; Sato, M.; Ruedy, R. Radiative forcing and climate response. *J. Geophys. Res.* **1997**, *102*, 6831–6864. [[CrossRef](#)]
5. Toon, O.B. How pollution suppresses rain. *Science* **2000**, *287*, 1763–1765. [[CrossRef](#)]
6. Rosenfeld, D. Aerosols, clouds, and climate. *Science* **2006**, *312*, 1323–1324. [[CrossRef](#)] [[PubMed](#)]
7. Rosenfeld, D. Suppression of rain and snow by urban and industrial air pollution. *Science* **2000**, *287*, 1793–1796. [[CrossRef](#)] [[PubMed](#)]
8. Rosenfeld, D. Aerosol-cloud interactions control of earth radiation and latent heat release budgets. *Sp. Sci. Rev.* **2006**, *125*, 149–157. [[CrossRef](#)]
9. Che, H.Z.; Shi, G.Y.; Zhang, X.Y.; Arimoto, R.; Zhao, J.Q.; Xu, L.; Wang, B.; Chen, Z.H. Analysis of 40 years of solar radiation data from China, 1961–2000. *Geophys. Res. Lett.* **2005**, *32*. [[CrossRef](#)]
10. Menon, S.; Hansen, J.E.; Nazarenko, L.; Luo, Y.F. Climate effects of black carbon aerosols in China and India. *Science* **2002**, *297*, 2250–2253. [[CrossRef](#)] [[PubMed](#)]
11. Collins, M.; Knutti, R.; Arblaster, J.; Dufresne, J.; Fichet, T.; Friedlingstein, P.; Gao, X.; Gutowski, W.; Johns, T.; Krinner, G. Contribution of working group I to the fifth assessment report of the intergovernmental panel on climate change. In *Climate Change 2013: The Physical Science Basis*; Qin, D., Plattner, G.K., Tignor, S.K.A., Judith, B., Alexander, N., Yu, X., Vincent, B., Pauline, M.M., Eds.; Cambridge University Press: Cambridge, UK, 2013; pp. 571–657.
12. Ramanathan, V.; Crutzen, P.J.; Kiehl, J.T.; Rosenfeld, D. Atmosphere—Aerosols, climate, and the hydrological cycle. *Science* **2001**, *294*, 2119–2124. [[CrossRef](#)] [[PubMed](#)]

13. McComiskey, A.; Feingold, G.; Frisch, A.S.; Turner, D.D.; Miller, M.A.; Chiu, J.C.; Min, Q.; Ogren, J.A. An assessment of aerosol-cloud interaction in marine stratus clouds based on surface remote sensing. *J. Geophys. Res.* **2009**, *114*, D09203. [[CrossRef](#)]
14. Forest, C.E.; Stone, P.H.; Sokolov, A.P.; Allen, M.R.; Webster, M.D. Quantifying uncertainties in climate system properties with the use of recent climate observations. *Science* **2002**, *295*, 113–117. [[CrossRef](#)] [[PubMed](#)]
15. Cattani, E.; Costa, M.J.; Torricella, F.; Levizzani, V.; Silva, A.M. The influence of the aerosol particles from biomass burning on cloud microphysical properties and radiative forcing. *Atmos. Res.* **2006**, *82*, 310–327. [[CrossRef](#)]
16. Anderson, T.L.; Charlson, R.J.; Schwartz, S.E.; Knutti, R.; Boucher, O.; *et al.* Climate forcing by aerosols—A hazy picture. *Science* **2003**, *300*, 1103–1104. [[CrossRef](#)] [[PubMed](#)]
17. Hansen, J.; Sato, M.; Ruedy, R.; Lacis, A.; Oinas, V. Global warming in the twenty-first century: An alternative scenario. *Proc. Natl. Acad. Sci. USA* **2000**, *97*, 9875–9880. [[CrossRef](#)] [[PubMed](#)]
18. Holben, B.; Tanre, D.; Smirnov, A.; Eck, T.; Slutsker, I.; Abuhassan, N.; Newcomb, W.W.; Schafer, J.; Chatenet, B.; Lavenue, F.; *et al.* An emerging ground-based aerosol climatology: Aerosol optical depth from AERONET. *J. Geophys. Res.* **2001**, *106*, 12067–12097. [[CrossRef](#)]
19. Holben, B.N.; Eck, T.F.; Slutsker, I.; Tanre, D.; Buis, J.P.; Setzer, A.; Vermote, E.; Reagan, J.A.; Kaufman, Y.; Nakajima, T.; *et al.* AERONET—A federated instrument network and data archive for aerosol characterization. *Remote Sens. Environ.* **1998**, *66*, 1–16. [[CrossRef](#)]
20. Goloub, P.; Li, Z.; Dubovik, O.; Blarel, L.; Podvin, T.; Jankowiak, I.; Lecoq, R.; Deroo, C.; Chatenet, B.; Morel, J.P.; *et al.* PHOTONS/AERONET sunphotometer network overview: Description, activities, results. *Proc. SPIE* **2007**, *6936*, 69360V.
21. Prats, N.; Cachorro, V.E.; Berjón, A.; Toledano, C.; De Frutos, A.M. Column-integrated aerosol microphysical properties from AERONET Sun photometer over southwestern Spain. *Atmos. Chem. Phys.* **2001**, *11*, 12535–12547. [[CrossRef](#)]
22. Bokoye, A.I.; Royer, A.; O'Neill, N.T.; Cliche, P.; Fedosejevs, G.; Teillet, P.M.; McArthur, L.J.B. Characterization of atmospheric aerosols across Canada from a ground-based sunphotometer network. *Aerocan. Atmos. Ocean.* **2001**, *39*, 429–456. [[CrossRef](#)]
23. Kim, D.H.; Sohn, B.J.; Nakajima, T.; Takamura, T.; Takemura, T.; Choi, B.C.; Yoon, S.C. Aerosol optical properties over east Asia determined from ground-based sky radiation measurements. *J. Geophys. Res.* **2004**, *109*. [[CrossRef](#)]
24. Uchiyama, A.; Yamazaki, A.; Togawa, H.; Asano, J. Characteristics of aeolian dust observed by sky-radiometer in the Intensive Observation Period 1 (IOP1). *J. Meteorol. Soc. Jpn.* **2005**, *83A*, 291–305. [[CrossRef](#)]
25. Pappalardo, G.; Amodeo, A.; Apituley, A.; Comerón, A.; Freudenthaler, V.; Linné, H.; Ansmann, A.; Bösenberg, J.; D'Amico, G.; Mattis, I.; *et al.* EARLINET: Towards an advanced sustainable European aerosol lidar network. *Atmos. Meas. Tech.* **2014**, *7*, 2389–2409. [[CrossRef](#)]
26. Guerrero-Rascado, J.L.; Landulfo, E.; Antuña, J.C.; Barbosa, H.M.J.; Barja, B.; Bastidas, A.E.; Bedoya, A.E.; Costa, R.; Estevan, R.; Forno, R.; *et al.* Latin American Lidar Network (LALINET) for aerosol research: Diagnosis on network instrumentation. *J. Atmos. Sol.-Terr. Phys.* **2016**. [[CrossRef](#)]
27. Welton, E.J.; Campbell, J.R.; Spinhirne, J.D.; Scott, V.S. Global monitoring of clouds and aerosols using a network of micro-pulse lidar systems. *Proc. SPIE* **2001**, *4153*. [[CrossRef](#)]
28. Che, H.; Zhang, X.Y.; Chen, H.B.; Damiri, B.; Goloub, P.; Li, Z.Q.; Zhang, X.C.; Wei, Y.; Zhou, H.G.; Dong, F.; *et al.* Instrument calibration and aerosol optical depth validation of the China aerosol remote sensing network. *J. Geophys. Res.* **2009**, *114*. [[CrossRef](#)]
29. Che, H.; Zhang, X.Y.; Xia, X.; Goloub, P.; Holben, B.; Zhao, H.; Wang, Y.; Zhang, X.C.; Wang, H.; Blarel, L.; *et al.* Ground-based aerosol climatology of China: Aerosol optical depths from the China aerosol remote sensing network (CARSNET) 2002–2013. *Atmos. Chem. Phys.* **2015**, *15*, 7619–7652. [[CrossRef](#)]
30. Tao, R.; Che, H.Z.; Chen, Q.L.; Wang, Y.Q.; Sun, J.Y.; Zhang, X.C.; Lu, S.; Guo, J.P.; Wang, H.; Zhang, X.Y. Development of an integrating sphere calibration method for Cimel sunphotometers in China aerosol remote sensing network. *Particuology* **2014**, *13*, 88–99. [[CrossRef](#)]
31. Che, H.Z.; Wang, Y.Q.; Sun, J.Y.; Zhang, X.C. Assessment of *In-situ* langley calibration of CE-318 sunphotometer at Mt. Waliguan Observatory, China. *SOLA* **2011**, *7*. [[CrossRef](#)]

32. Che, H.; Xia, X.; Zhu, J.; Li, Z.; Dubovik, O.; Holben, B.; Goloub, P.; Chen, H.; Estelles, V.; Cuevas-Agulló, E.; *et al.* Column aerosol optical properties and aerosol radiative forcing during a serious haze-fog month over North China Plain in 2013 based on ground-based sunphotometer measurements. *Atmos. Chem. Phys.* **2014**, *14*, 2125–2138. [[CrossRef](#)]
33. Yu, J.; Che, H.Z.; Chen, Q.L.; Xia, X.A.; Zhao, H.J.; Wang, H.; Wang, Y.Q.; Zhang, X.Y.; Shi, G.Y. Investigation of aerosol optical depth (AOD) and Ångström exponent over the desert region of Northwestern China based on measurements from the China aerosol remote sensing network. *Aerosol. Air. Qual. Res.* **2014**, *15*, 2024–2036. [[CrossRef](#)]
34. Zhao, H.J.; Che, H.Z.; Ma, Y.J.; Xia, X.A.; Wang, Y.F.; Wang, P.; Wu, X.C. Temporal variability of the visibility, particulate matter mass concentration and aerosol optical properties over an urban site in Northeast China. *Atmos. Res.* **2015**, *166*. [[CrossRef](#)]
35. Xia, X.; Che, H.; Zhu, J.; Chen, H.; Cong, Z.; Deng, X.; Fan, X.; Fu, Y.; Goloub, P.; Jiang, H.; *et al.* Ground-based remote sensing of aerosol climatology in China: Aerosol optical properties, direct radiative effect and its parameterization. *Atmos. Environ.* **2015**, *124*. [[CrossRef](#)]
36. Kaufman, Y.J.; Gitelson, A.; Karnieli, A.; Ganor, E.; Fraser, R.S.; Nakajima, T.; Mattoo, S.; Holben, B.N. Size distribution and scattering phase function of aerosol particles retrieved from sky brightness measurements. *J. Geophys. Res.* **1994**, *99*. [[CrossRef](#)]
37. Eck, T.F.; Holben, B.N.; Reid, J.S.; Dubovik, O.; Smirnov, A.; O'Neill, N.T.; Slutsker, I.; Kinne, S. Wavelength dependence of the optical depth of biomass burning, urban, and desert dust aerosols. *J. Geophys. Res.* **1999**, *104*, 31333–31349. [[CrossRef](#)]
38. Wagner, F.; Silva, A.M. Some considerations about Angström exponent distributions. *Atmos. Chem. Phys.* **2008**, *8*, 481–489. [[CrossRef](#)]
39. Zhang, R.; Jing, J.; Tao, J.; Hsu, S.-C.; Wang, G.; Cao, J.; Lee, C.S.L.; Zhu, L.; Chen, Z.; Zhao, Y.; *et al.* Chemical characterization and source apportionment of PM_{2.5} in Beijing: Seasonal perspective. *Atmos. Chem. Phys.* **2013**, *13*, 7053–7074. [[CrossRef](#)]
40. Dubovik, O.; King, M.D. A flexible inversion algorithm for the retrieval of aerosol optical properties from Sun and sky radiance measurements. *J. Geophys. Res.* **2000**, *105*, 673–696. [[CrossRef](#)]
41. Dubovik, O.; Smirnov, A.; Holben, B.N.; King, M.D.; Kaufman, Y.J.; Eck, T.F.; Slutsker, I. Accuracy assessments of aerosol optical properties retrieved from AERONET sun and sky radiance measurements. *J. Geophys. Res.* **2000**, *105*, 9791–9806. [[CrossRef](#)]
42. Dubovik, O.; Sinyuk, A.; Lapyonok, T.; Holben, B.N.; Mishchenko, M.; Yang, P.; Eck, T.F.; Volten, H.; Munoz, O.; Veihelmann, B.; *et al.* Application of spheroid models to account for aerosol particle nonsphericity in remote sensing of desert dust. *J. Geophys. Res. Atmos.* **2006**, *111*. [[CrossRef](#)]
43. Kasten, F. A new table and approximate formula for relative optical air mass. *Arc. Meteorol. Geophys. Bio.* **1966**, *14*, 206–233. [[CrossRef](#)]
44. Kasten, F.; Young, A.T. Revised optical air mass tables and approximation formula. *Appl. Opt.* **1989**, *28*, 4735–4738. [[CrossRef](#)] [[PubMed](#)]
45. Komhyr, W.D.; Mateer, C.L.; Hudson, R.D. *Operations Handbook—Ozone Observations with A Dobson Spectrophotometer*; Report No.6; WMO Global Ozone Research and Monitoring Project: Geneva, Switzerland, 1980.
46. Fröhlich, C.; Shaw, G.E. New determination of Rayleigh scattering in the terrestrial atmosphere. *Appl. Opt.* **1980**, *19*, 1773–1775. [[CrossRef](#)] [[PubMed](#)]
47. Thome, K.J.; Herman, B.M.; Reagan, J.A. Determination of precipitable water from solar transmission. *J. Appl. Meteorol.* **1992**, *31*, 157–165. [[CrossRef](#)]
48. Paltridge, G.W.; Platt, C.M.R. Radiative processes in meteorology and climatology. *Dev. Atmos. Sci.* **1976**, *5*. [[CrossRef](#)]
49. Smirnov, A.; Holben, B.N.; Eck, T.F.; Dubovik, O.; Slutsker, I. Cloud-screening and quality control algorithms for the AERONET database. *Remote. Sens. Environ.* **2000**, *73*, 337–349. [[CrossRef](#)]

